Fine tuning of pattern selection in the cadmium–hydroxide-system

Paszkál Papp,[1] Bíborka Bohner,[1] Ágota Tóth,[1] and Dezső Horváth[2, a)]

[1)] *Department of Physical Chemistry and Materials Science, University of Szeged, Rerrich Béla tér 1., Szeged, H-6720, Hungary*

[2)] *Department of Applied and Environmental Chemistry, University of Szeged, Rerrich Béla tér 1., Szeged, H-6720, Hungary*

(Dated: 18 February 2020)

Controlling self-organization in precipitation reactions has received growing attention in the efforts of engineering highly ordered spatial structures. Experiments have been successful in regulating the band patterns of the Liesegang phenomenon on various scales. Herein we show that by adjusting the composition of the hydrogel medium we can switch the final pattern between the classical band structure and the rare precipitate spots with hexagonal symmetry. The accompanying modeling study reveals that besides the modification of gel property, the tuning of the time scale of diffusional spreading of hydroxide ion with respect to that of the phase separation drives the mode selection between one-dimensional band and two-dimensional spot patterns.

[a)] E-mail: horvathd@chem.u-szeged.hu

I. INTRODUCTION

Self-organization and dynamic self-assembly are responsible for creating complex patterns that surround us both in the animate and inanimate world.[1,2] Positive feedback within the underlying mechanism plays the essential role in the local decrease in entropy that is associated with the generation of highly ordered structures far from thermodynamic equilibrium. In chemical systems when diffusion is coupled to homogeneous reaction kinetics, nonlinearity may lead to various spatiotemporal concentration patterns: for example, waves of excitation[2], autocatalytic fronts[3,4], or stationary Turing patterns[5,6].

In heterogeneous reactions, the growth of solid particles inherently contains the necessary feedback, therefore precipitate reactions may result in nontrivial spatial structures[7,8]. In case of Liesegang patterns the externally imposed concentration gradient of one of the components in an appropriately chosen hydrogel medium drives a reaction that leads to periodic zones of precipitates: orderly spaced bands in a one-dimensional configuration and rings in a two-dimensional[9–12]. A series of mathematical formulae to describe this periodic and/or monotonic spatial distribution of the precipitate stripes—spacing law[13], width law[14], time law[15], and the Matalon–Packter-law[16]—are associated with the stationary structures that originate from the temporal evolution of the governing concentration gradients[17]. Two general descriptions have been proposed in the explanation of the phenomenon, pre-nucleation[18–22] and post-nucleation[23–25] models, both of which can account for the various experimental observations: control of spacing by external electric field[26,27], formation of defects in transverse direction due to thermal fluctuations, and evolution of helical bands[28] or fractal structures[29]. The applicability of these precipitate structures by downsizing in micro- and nanotechnology has given them recent interest where engineering the patterns are seen as the ultimate goal. Wet stamping has successfully been applied in creating microscale patterns[30,31], aggregation of nanoparticles shows resemblance to Liesegang patterns[32], controlled engineering has been attempted by introducing impurities in the hydrogel medium[33], by allowing complex formation[34], by increasing hydrophobicity of the gel at low temperature[35], and by employing an external magnetic field[36].

Beyond bands and their variants, unique spot structure with square and hexagonal symmetry has been found by Dayen et al.[37] in the cadmium–sulfide system where they have also shown that the band-to-spot transition can be triggered by varying the inner electrolyte

concentration. Unlike in the classical setup where the solution containing the cation of the precipitate takes the role of the outer electrolyte to avoid complexation and partial dissolution of the structure[38], they have allowed sodium sulfide to diffuse into a hydrogel loaded with cadmium chloride. The key process is the formation of cadmium hydroxide precipitate in the basic solution followed by an ion-exchange reaction yielding cadmium sulfide, however, the latter does not modify the spatial structure of the pattern. Hence the fast diffusing hydroxide ion may have been responsible for the unusual appearance of spots.

In this work we focus on the mode selection between the spotted and banded patterns by carrying out experiments in the reaction between cadmium and hydroxide ions. We show the importance of the time scale of diffusional spreading for hydroxide ion which can be controlled by carefully varying the amount of carboxylic groups—used as binders—within the hydrogel medium. This technique has been succesfully exploited in nonlinear systems to induce long range inhibition that resulted in Turing patterns[6] or transverse front instability[4,39]. Parallel with the experiments, we construct a model by coupling the reaction–diffusion system incorporating the reversible binding with the spinodal decomposition driving the phase separation to recapture the observed spot-to-band transitions with increasing binding.

II. EXPERIMENTAL STUDY

Solutions were prepared via accurate weighing of analytical-grade cadmium chloride (Reanal) and sodium hydroxide (Spektrum-3D). To synthesize the poly(acrylamide-co-methacrylic acid) hydrogel, the cross-linking agent N,N'-methylenebisacrylamide (0.1 g) was first dissolved in 10 ml warm deionized water, followed by the addition of 3.0 g acrylamide monomer to the solution. Subsequently, 0.3 ml 30 V/V% triethanolamine (Reanal), and sodium methacrylate—made from equal amount of methacrylic acid ((MAA) Aldrich) and sodium hydroxide—were added to the vigorously stirred homogenous solution. The mixture was then placed in an ice–water bath and the system was evacuated via employing a water-jet pump for 30 minutes to minimize dissolved oxygen. Finally, 1 cm^3 (0.055 mol/dm^3) potassium persulfate (Reanal) initiator was added to the system, resulting in a solution of 15 cm^3 in total. The highly viscous solution was allowed to solidify for 30 minutes in a pre-formed, 1-mm-thick template made of Plexiglas, into which the reaction mixture was transferred with a syringe. The unreacted monomer molecules from the synthesized gel

were removed by soaking and rinsing the prepared gel repeatedly in deionized water. To protonate the carboxylate groups in the hydrogel, the sheets were soaked in a hydrochloric acid solution, followed by rinsing with deionized water. Finally, the gel sheets with the acidic form of MAA were impregnated in $0.06 - 0.08$ mol/dm^3 cadmium chloride solutions. Because the gel sheets shrank and swelled at various stages of the preparation, they were precisely cut to form with a rotary cutter only after the loading of the reactant solution.

Several two-dimensional geometric arrangements have been considered as reaction media. In the preliminary experiments horizontally oriented circular gels were sandwiched between Plexiglas plates. The top plate had a circular opening in the center, where the outer electrolyte came into contact with the gel. Systematic experiments were then performed in vertically oriented rectangular and trapezoidal gels positioned between Plexiglas plates and adjustable side spacers. As the reactor was assembled, the plates formed an open reservoir above the gel upper edge. The application of a thin film of vaseline ensured the prevention of gel dehydration and the leakage of the outer electrolyte. Once sodium hydroxide solution was filled in the reservoir to initiate the reaction, the assembly was covered with an adhesive tape to minimize evaporation.

Experiments were carried out in a controlled-temperature refrigerator equipped with a transparent door at 20±1 °C. The gel sheets were illuminated with a white LED light source operated by a relay synchronized with a camera. Gray scale images of the developing precipitate structure in front of a black background were taken in every 10 minutes with a digital camera (Unibrain, Sony).

In-house software was used for analyzing the geometrical descriptors—position and width—of the evolved precipitate patterns. Quantitative characterization was carried out on three parallel, randomly selected areas along the spreading of the outer electrolyte. Location of gray scale maxima defined the position of the white precipitate bands, while the width of each band was given by the distance between the neighboring points of inflection.

The microstructure of the formed crystals in the gel was studied by employing a scanning electron microscope (SEM, Hitachi S-4700 operated in the 10–20 kV acceleration voltage range). Prior to the SEM measurements, a freeze-drying process was used to completely remove the water content of the hydrogel. The dry samples were then secured carefully on a double-sided adhesive carbon tape, and coated with gold–platinum alloy for 30 seconds using a sputter coater (Quorum Technologies SC7620). Control batch experiments were

also performed to check the phase composition of the precipitates forming under identical reactant concentrations but in the absence of gel.

III. EXPERIMENTAL RESULTS AND DISCUSSION

In our experiments the gel has a two-fold role: it hinders convection as in the case of classical Liesegang-ring formation, and it allows the fine tuning of the diffusional rate for the outer electrolyte sodium hydroxide solution. By varying the amount of methacrylic acid groups in the hydrogel, we can control the diffusion of hydroxide ion as it first has to deprotonate methacrylic groups bound in the polymer matrix according to

$$\text{M-COOH(gel)} + \text{OH}^- \rightleftharpoons \text{M-COO}^-\text{(gel)} + \text{H}_2\text{O} \tag{1}$$

with the equilibrium constant in the order of 10^9 considering the acidity of small carboxylic acids.[4] This reaction is then coupled to the main precipitation forming reaction of

$$\text{Cd}^{2+} + 2\text{OH}^- \rightleftharpoons \text{Cd(OH)}_2\text{(s)} \tag{2}$$

with a solubility product[40] of 4.5×10^{-15}. Upon setting the constant concentration of 0.06 mol/dm^3 for the cadmium chloride inner electrolyte and 0.4 mol/dm^3 for the sodium hydroxide solution, we vary the MAA content of the gel and let the outer electrolyte diffuse from a center source.

In the assembly with circular gel, stationary concentric precipitate rings evolve that have the tendency of breaking into segments at larger diameter (see Fig. 1). At these defects a phase shift of $\pi/2$ develops, i.e., precipitate zone arises on one side and precipitate free zone on the other. With increasing MAA content, the breaking up of the rings becomes dominant and the classical rings are replaced with a spotted pattern similar to that observed in the cadmium-sulfide system[37]. However, at 55.0 mmol/dm^3 MAA concentration, the spots abruptly disappear and the concentric rings evolve again. We have repeated the experiments in rectangular and trapezoid gel sheets with planar source and observed only band formation which indicates that curvature in general enhances spot formation.

Quantitative analysis of the position of the precipitate bands (x_i) reveals that they follow the classical spacing law, i.e., a unique spacing coefficient ($P = x_{i+1}/x_i$) exists, yielding a constant ratio for the distance of adjacent bands from the contact line of the outer electrolyte.

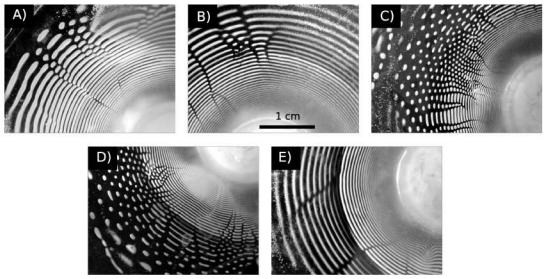

FIG. 1. Cadmium hydroxide precipitate pattern in a circular geometry with [$CdCl_2$(gel)] = 0.06 mol/dm^3, [NaOH] = 0.4 mol/dm^3, [MAA] = 23.6 (A), 31.4 (B), 39.3 (C), 47.2 (D), and 55.0 mmol/dm^3 (E). The scale bar is the same for all images.

The spacing coefficient, determined by fitting the function of $x_i = x_0 P^i$ with x_0 being the position of the first visible band, remains constant (1.05±0.04) within experimental errors independently of the gel geometry even when the concentration of MAA in the gel is increased. The width law coefficient ($Q = w_{i+1}/w_i$) can only be obtained with larger uncertainty (10–20 %) because of the spatial resolution of the acquired images. For our conditions Q is estimated in the range of 1.02–1.04 that satisfies the general relation of $Q < P$ valid for most Liesegang patterns. The appearance of consecutive bands scales with x_i^2 matching the time law, which indicates that diffusive spreading drives the precipitate reaction.

Here we focus on the spot–band transition with increasing MAA concentration in the gel, therefore we increase the cadmium chloride concentration to 0.08 mol/dm^3 to favor spot formation. The domain of cadmium hydroxide precipitate spots shifts to higher MAA content although it still only represents a 5-6 % binding of the diffusing hydroxide ion, but at the same time it now appears for a planar source as well, as shown in Figs. 2 and 3. At the highest selected MAA concentration we observe the reappearance of the band pattern for each reactor geometry. It is important to note that the gradual transverse widening of the trapezoid hydrogel favors the segmentation of the precipitate bands because the range of precipitate spots is wider and more enhanced in the trapezoid configuration compared to the rectangular one. The continuous segmentation results in a growing number of defects that form grain boundaries with a $\pi/2$ phase shift that finally leads to regular spotted pattern arranged in a hexagonal symmetry. Along the direction of propagation these precipitate

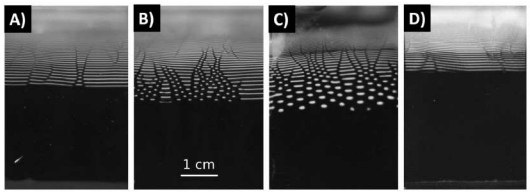

FIG. 2. Cadmium hydroxide precipitate pattern in a rectangular geometry with $[CdCl_2(gel)]$ = 0.08 mol/dm^3, [NaOH] = 0.4 mol/dm^3, [MAA] = 62.9 (A), 70.7 (B), 78.6 (C), and 86.5 mmol/dm^3(D). The scale bar is the same for all images.

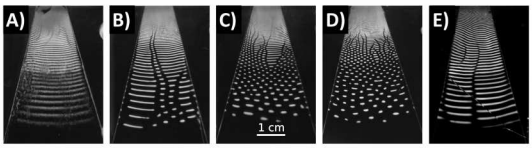

FIG. 3. Cadmium hydroxide precipitate pattern in a trapezoid geometry with $[CdCl_2(gel)]$ = 0.08 mol/dm^3, [NaOH] = 0.4 mol/dm^3, [MAA] = 55.0 (A), 62.9 (B), 70.7 (C), 78.6 (D), and 86.5 mmol/dm^3(E). The scale bar is the same for all images.

patterns are also characterized with the same space coefficient within experimental errors, i.e., $P = 1.05 \pm 0.01$ in case of the rectangular cell in the entire range of MAA content.

By measuring the black and white pixels in the experimental images, we can calculate the coverage of the final pattern; while the precipitate bands occupy 20% of the reaction medium, cadmium hydroxide spots only cover 10% of the gel sheet. This characterizes both the rectangular and the trapezoid gel medium.

Regarding the morphology of the precipitates, profound differences exist between those formed in the well-stirred control experiment and in the gel system. In the former, oblong-shaped crystals with sharp edges and clearly visible facets are produced, with an average length of ~ 10 μm as shown in Fig. 4(A). In the gel medium, mainly amorphous spherical particles appear both within the spots (Fig. 4(B)) and in the precipitate bands (Fig. 4(C)) with diameters of ~ 0.5 μm. While the bands are made up of densely packed precipitate particles, the depletion zones between them contain significantly less number of cadmium hydroxide particles with diameters approximately third of those present within the bands.

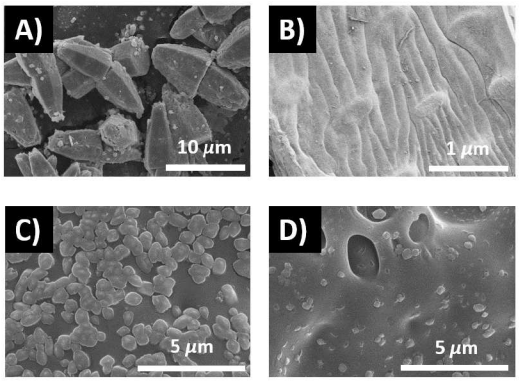

FIG. 4. SEM image of cadmium hydroxide crystals formed in the well-stirred system (A), in a spot (B), within a precipitate-rich band (C), and in the depletion zone between bands (D).

IV. MODELING STUDY

Our reaction-diffusion model is based on the coupling of the fast reversible binding of hydroxide ion in the hydrogel and the reaction between cadmium and hydroxide ions to produce a colloidal intermediate that in turn yields the final precipitate according to

$$\mathrm{A} + \mathrm{HX} \rightleftharpoons \mathrm{X} \tag{3a}$$

$$2\mathrm{A} + \mathrm{B} \longrightarrow \mathrm{C} \tag{3b}$$

$$\mathrm{C} \longrightarrow \mathrm{D} \tag{3c}$$

Equation (3a) corresponds to Eq. (1) where HX represents the carboxylic acid groups within the gel that removes free hydroxide ions (A). Equation (2) is divided into two steps: first cadmium ions (B) in the presence of hydroxide ions are converted into the insoluble cadmium hydroxide which we first treat as a colloidal intermediate (C) that yields the final product (D) in the subsequent step that represent the actual precipitate $Cd(OH)_2(s)$.

We consider that the intermediate with the solvent constitutes a non-ideal solution allowing spontaneous phase separation via spinodal decomposition, resulting in regions of low and high intermediate concentration that in the end appear as precipitate lean and rich

areas. In dimensionless form the governing differential equations of the system are

$$\frac{\partial a}{\partial t} = \frac{1}{s}\left(D_a \nabla^2 a \; - \; 2\, k_1\, a\, b\right) \tag{4a}$$

$$\frac{\partial b}{\partial t} = D_b \nabla^2 b \; - \; k_1\, a\, b \tag{4b}$$

$$\frac{\partial \varphi}{\partial t} = -\lambda \nabla^2 \left(\varepsilon\varphi - \beta\varphi^2 - \gamma\varphi^3 + \sigma\nabla^2\varphi\right) + k_1 F_1\, a\, b \; - k_2\left(\varphi + F_2\right) \tag{4c}$$

$$\frac{\partial d}{\partial t} = k_2 \frac{\varphi + F_2}{F_1} \tag{4d}$$

where a, b, and d are the dimensionless concentrations of A, B, and D, respectively, scaled to the standard concentration, while D_a and D_b are the corresponding diffusion coefficients. The solid cadmium hydroxide precipitate is immobile, therefore its diffusion coefficient is zero. The first term in Eq. (4c) is from the Cahn–Hilliard equation[41] that contains the Gibbs energy functional according to an asymmetric Ginzburg–Landau equation. For the sake of simplicity, we use rescaled intermediate concentration $\varphi = F_1\, c - F_2$ where the additional scaling is based on the coefficients of the Cahn–Hilliard equation (γ, β and σ) as

$$F_1 = \frac{\sqrt{4\varepsilon\gamma + \beta^2}}{\gamma\left(c_h - c_l\right)} \tag{5a}$$

$$F_2 = \frac{\sqrt{4\varepsilon\gamma + \beta^2}(c_h + c_l)}{2\gamma(c_h - c_l)} + \frac{\beta}{2\gamma} \tag{5b}$$

with c_l and c_h being the concentration of intermediate following the phase separation, i.e., the concentration at the Gibbs energy minima. The extent of hydroxide ion removal in Eq. (4a) is expressed as

$$s = 1 + \frac{c_x K}{(K + a)^2}, \tag{6}$$

where c_x corresponds to the total concentration of immobile binder groups in the gel and K is defined as the equilibrium constant associated with the reverse reaction of Eq. (1) in accordance with previous treatments of reversible binding in hydrogels[4]. The importance of parameter s is that D_a/s can be considered as the effective diffusion coefficient for hydroxide ion. For strong binding ($K \ll 1$) at the leading edge of the diffusional front $s \gg 1$, while it decreases to 1 behind the front.

The partial differential equations of Eq. (4) are solved on either a 1000×1000 square or a 500×1000 rectangle two dimensional grid by a finite difference method, where the grid spacing is set to 0.1 using no-flux boundary condition. The ∇^2 operator is approximated

with a nine-point, while the ∇^4 operator with a twenty-five-point discretized formula. For the calculations, the CVODE[42] solver with the Backwards Differentiation Formula (BDF) is selected from the SUNDIALS[43] package, with the code running in parallel using the openMPI implementation of Message Passing Interface (MPI). The initial dimensionless concentrations relative to the standard concentration are $a = 0.4$, $b = 0.06$ according to the experiments. The dimensionless diffusion coefficients relative to that of hydroxide ion are $D_a = 1.0$, $D_b = 0.2$. The scaling parameters c_h and c_l, and the asymmetry coefficient β are set to obtain precipitate coverage corresponding to the experimental observations. Among the coefficients of the Cahn–Hilliard equation λ is set to match the spatial dimensions, i.e., widths of precipitate bands vs. distance between them, to the experimental observations, ϵ and γ are adjusted so that the system is in the vicinity of the pattern transition. Hence we select $c_h = 0.158$, $c_l = 10^{-5}$, $\lambda = 0.01$, $\epsilon = 1.0$, $\gamma = 0.2$, $\beta = -2.25$ and $\sigma = 0.04$, while $k_1 = 1.0$, $k_2 = 0.01$ are used for rate coefficients. For this grid to decrease computational time we can set $K = 0.01$ which is greater than the experimental value because the system is insensitive to it as long as $K \ll 1$ remains valid. Thermal fluctuations are introduced in the system by applying an initial random perturbation with an amplitude of 0.2 in φ. Two types of initialization are considered in our study: one with a planar source and one with a point source.

V. MODELING RESULTS AND DISCUSSION

In spinodal decomposition governed by the Cahn–Hilliard equation, the coefficient λ sets the characteristic length scale of the final pattern. During the preliminary calculations we have adjusted its value to match the relative coverage of the state with high concentration of D to those of the precipitate bands in the experiments. The coefficient σ in Eq. (4c) acts as surface tension: the greater it is, the shorter is the boundary between the two states to which separation takes place. Namely, large σ favors the formation of bands, while small σ can lead to patterns with spots. Even though parameter σ depends on the structure of the hydrogel, its experimental control is not a straightforward task. In order to capture the experimental observations in our numerical study, we have therefore set σ to a medium value and vary the amount of immobile binder (c_x).

Figure 5 depicts the resultant patterns visualized by the concentration field of the final

product D. The initial bands break up into spots for $c_x \leq 0.08$, while the band structure is stable for $c_x > 0.08$. The band-to-spot transition seen at greater MAA content in the experiments is recaptured by the modeling results. Similar transition is observed when

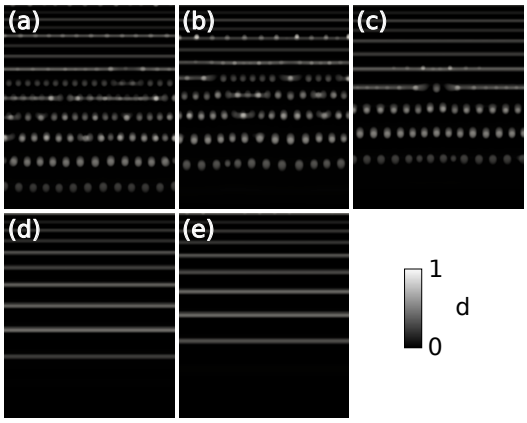

FIG. 5. The effect of increasing binder concentration ($c_x = 0.00$ (a), 0.04 (b), 0.08 (c), 0.12 (d), 0.16 (e)) on the patterns obtained in a rectangular geometry with component A diffusing through the upper boundary constituting a line source.

component A diffuses from a point source. The circular pattern arising for $c_x \geq 0.08$ is, however, a linear combination of the spotted and banded pattern because in the outer bands there is an angular variation in the final amount of D.

The increase in the binder concentration does not affect the final product concentration. Because component A corresponding to the hydroxide ions is in large stoichiometric excess, it turns the entire inner eletrolyte (containing the cadmium ion) into intermediate C. If we do not consider phase separation, the concentration of the intermediate behind the diffusional spreading of the hydroxide varies only negligibly with increasing amount of binder, as shown in Fig. 7. The figure also reveals that the increase in the binder concentration slows down the propagation of the outer electrolyte because the fast deprotonation of the carboxylic acid groups decreases the amount of free hydroxide ions at the leading edge and, hence, hinders their spatial spreading. Independently of the deprotonation equilibrium, the propagation scales with the square root of time (see Fig. 8) as expected for diffusional fronts.

The slowing down of the front is sufficient for driving the spot-to-band transition in the

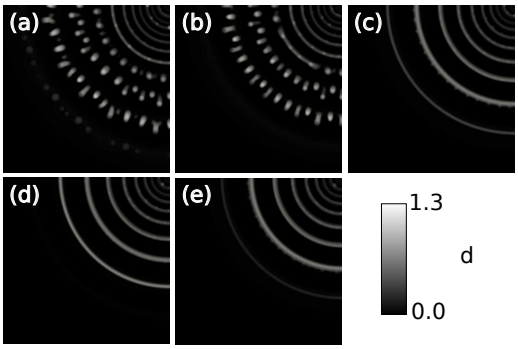

FIG. 6. The effect of increasing binder concentration ($c_x = 0.00$ (a), 0.04 (b), 0.08 (c), 0.12 (d), 0.16 (e)) on the patterns obtained in a square geometry with component A diffusing from the upper right corner constituting a small circular source.

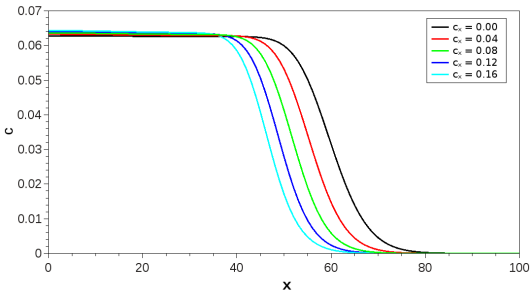

FIG. 7. The invariant intermediate concentration behind the diffusional front with increasing binder concentration for $a_0 = 0.06$ at $t = 1000$.

precipitate formation, which can be rationalized by considering the characteristic times associated with the diffusional front propagation and the phase separation. At the selected reactant concentrations, independently of the binding, the reaction in Eq. (3b) builds up an intermediate concentration that falls inside the unstable region where spontaneous spinodal decomposition can take place. With more binder ($c_x > 0.08$), the gradient along the propagation decays slower, hence it can create a longer lasting directional perturbation that is superimposed on the thermal fluctuations driving the phase separation. In the resultant patterns the concentration gradients are amplified along the diffusional direction, while they

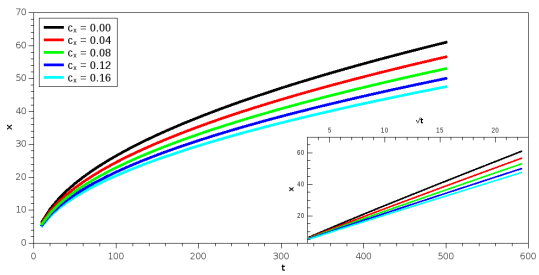

FIG. 8. Front evolution with increasing binder component concentration.

vanish perpendicular to it, giving rise to precipitate bands. With less binder, on the other hand, the faster diffusional spreading leaves behind an unstable region of intermediate where the faster decaying concentration gradient in the direction of propagation does not dominate any more. Thermal fluctuations amplify the concentration gradients in both direction during phase separation and spotted precipitate pattern is the result. When a point source is applied instead of a planar one the diffusional front enters a region expanding transversely that brings in an additional perturbation, hence spotted pattern is more favorable. The change in the relation of time scales—diffusional spreading and phase separation—with increasing binder content does not explain, however, the band-to-spot transition observed experimentally at low MAA concentration. In the numerical study we can obtain pure banded patterns for $c_x = 0$ with different initial concentrations or different coefficients of the Cahn–Hilliard equation, however, we have not been able to reproduce a band-to-spot transition for those parameters by simply increasing c_x. Since in the experiments precipitate spots replace bands as the MAA is introduced in the hydrogel, that transition at low MAA concentration can be attributed to changes in the hydrogel structure with the introduction of carboxylic groups that changes the swelling properties, for example, which indirectly may cause changes in the coefficients of the Cahn–Hilliard equation in Eq. (4c).

VI. CONCLUSION

We have shown experimentally that by controlled modification of the hydrogel medium, we can tune the diffusional time scale of free hydroxide ion, one of the components in the reaction leading to precipitate patterns of cadmium hydroxide. As the amount of carboxylic

acid in the gel is increased two transitions are observed: first the classical Liesegang-type banded precipitate structure is replaced by a unique spotted pattern with hexagonal symmetry, then banded structure reappears again. The band-to-spot switch at low MAA content is attributed to a change in the gel properties that are known to be important in the formation of Liesegang patterns, while the spot-to-band switch is a result of the fine adjustment of the related times scales. Below a critical MAA content, the faster diffusional spreading of hydroxide ions leaves behind an unstable homogeneous distribution of colloidal cadmium hydroxide which leads to phase separation because of the inherent thermal fluctuations. The resultant precipitate pattern reflects the geometry of the domain, e.g., a layer of spots appears in a thin gel sheet. By slowing down the propagation of hydroxide ions with further increase in the amount of MAA, the concentration gradient along the propagation prevails longer and it represents an additional perturbation to the noise. Hence phase separation only takes place in the direction of propagation yielding a band structure even though the systems reaches the same unstable region. The transition to one-dimensional pattern can be hindered by allowing perturbations in transverse direction, for example, expanding the domain orthogonal to the direction of propagation. In the appropriately oriented trapezoidal gel sheet, therefore, the formation of spotted pattern is favored similarly to the case of a circular gel sheet around a point source. The spot-to-band transition have been reproduced in a reaction-diffusion model coupled to the spinodal decomposition of the intermediate state as the increase of binder resulted in the slow down of the diffusional spreading. The presented reversible binding with an active medium can now be considered as a successful tool in engineering spatial patterns beyond homogeneous systems where it is known to have the ability to spatially decouple the components and to form scenarios of long range inhibition with short range activation.

ACKNOWLEDGMENTS

The authors gratefully acknowledge Ádám Balog for carrying out some preliminary experiments and Dr. Gábor Schuszter for making the SEM images. This work was supported by the National Research, Development and Innovation Office (K119795) and GINOP-2.3.2-15-2016-00013 projects. P. Papp and B. Bohner thank the New National Excellence Programs (ÚNKP-18-1 and ÚNKP-16-3) for the financial support.

REFERENCES

[1]C. R. Kapral and K. Showalter, *Chemical Patterns and Waves* (Kluwer, Dordrecht, 1995).

[2]I. R. Epstein and J. A. Pojman, *An Introduction to Nonlinear Dynamics: Oscillations, Waves, Patterns, and Chaos* (Oxford University Press, Oxford, 1998).

[3]L. Szirovicza, I. Nagypál, and E. Boga, J. Am. Chem. Soc. **111**, 2842 (1989).

[4]D. Horváth and Á. Tóth, J. Chem. Phys. **108**, 1447 (1998).

[5]A. M. Turing, Philos. Trans. Roy. Soc. London B **237**, 37 (1952).

[6]V. Castets, E. Dulos, J. Boissonade, and P. De Kepper, Phys. Rev. Lett. **64**, 2953 (1990).

[7]I. Lagzi, ed., *Precipitation patterns in reaction-diffusion systems* (Research Signpost, India, 2010).

[8]E. Nakouzi and O. Steinbock, Sci. Adv. **2**, e1601144 (2016).

[9]R. E. Liesegang, Naturwissenschaftliche Wochenschrift **11**, 353 (1896).

[10]M. M. Ayass, M. Al-Ghoul, and I. Lagzi, J. Phys. Chem. A **118**, 11678 (2014).

[11]M. Matsue, M. Itatani, Q. Fang, Y. Shimizu, K. Unoura, and H. Nabika, Langmuir **34**, 11188 (2018).

[12]M. Itatani, Q. Fang, K. Unoura, and H. Nabika, J. Phys. Chem. C **122**, 3669 (2018).

[13]K. Jablczinsky, Bull. Soc. Chim. Fr. **33**, 1952 (1923).

[14]S. C. Müller, S. Kai, and J. Ross, J. Phys. Chem. **86**, 4078 (1982).

[15]H. W. Morse and G. W. Pierce, Proc. Am. Acad. Arts Sci. **38**, 623 (1903).

[16]R. Matalon and A. Packter, J. Colloid Sci. **10**, 46 (1955).

[17]H. Nabika, Curr. Phys. Chem. **5**, 5 (2015).

[18]C. Wagner, J. Colloid Sci. **5**, 85 (1950).

[19]J. B. Keller and S. I. Rubinow, J. Chem. Phys. **74**, 5000 (1981).

[20]G. Venzl, J. Chem. Phys. **85**, 1996 (1986).

[21]A. A. Mansour and M. Al-Ghoul, J. Phys. Chem. A **119**, 9201 (2015).

[22]A. Arango-Restepo, D. Barragán, and J. M. Rubi, Phys. Chem. Chem. Phys. **20**, 4699 (2018).

[23]R. Feeney, S. L. Schmidt, P. Strickholm, J. Chandam, and P. Ortoleva, J. Chem. Phys. **78**, 1293 (1983).

[24]G. Venzl, J. Chem. Phys. **85**, 2006 (1986).

[25]Z. Rácz, Physica A **274**, 50 (1999).

[26]I. Lagzi, Phys. Chem. Chem. Phys. **4**, 1268 (2002).

[27]I. Bena, M. Droz, I. Lagzi, K. Martens, Z. Rácz, and A. Volford, Phys. Rev. Lett. **101**, 075701 (2008).

[28]S. Thomas, I. Lagzi, F. Molnár Jr., and Z. Rácz, Phys. Rev. Lett. **110**, 078303 (2013).

[29]A. Toramaru, T. Harada, and T. Okamura, Physica D **183**, 133 (2003).

[30]M. Fialkowski, A. Bitner, and B. A. Grzybowski, Phys. Rev. Lett. **94**, 018303 (2005).

[31]I. T. Bensemann, M. Fialkowski, and B. A. Grzybowski, J. Phys. Chem. B **109**, 2774 (2005).

[32]I. Lagzi, B. Kowalczyk, and B. A. Grzybowski, J. Am. Chem. Soc. **132**, 58 (2010).

[33]I. Lagzi, Langmuir **28**, 3350 (2012).

[34]H. Nabika, M. Sato, and K. Unoura, Langmuir **30**, 5047 (2014).

[35]J. Jiang and K. Sakurai, Langmuir **32**, 9126 (2016).

[36]H. H., S. Aoki, and H. Abe, ACS Omega **3**, 4494 (2018).

[37]M. Dayeh, M. Ammar, and M. Al-Ghoul, RSC Adv. **4**, 60034 (2014).

[38]M. Saad, A. Safieddine, and R. Sultan, J. Phys. Chem. A **122**, 6043 (2018).

[39]Á. Tóth, I. Lagzi, and D. Horváth, J. Phys. Chem. **100**, 14837 (1996).

[40]S. Kotrlý and L. Šůcha, *Handbook of chemical equilibria in analytical chemistry* (Ellis Horwood Limited, England, 1985).

[41]J. Cahn and J. Hilliard, J. Chem. Phys. **28**, 258 (1958).

[42]S. D. Cohen and A. C. Hindmarsh, Comput. Phys. **10**, 138 (1996).

[43]A. C. Hindmarsh, P. N. Brown, K. E. Grant, S. L. Lee, R. Serban, D. E. Shumaker, and C. S. Woodward, ACM Trans. Math. Software **31**, 363 (2005).